BIOCHEMISTRY

A bacterial spermidine biosynthetic pathway via carboxyaminopropylagmatine

Huachao Xi[1,2], Xiaoqun Nie[1]*, Fang Gao[1], Xinxin Liang[3], Hu Li[1,2], Haiyan Zhou[1,2], Yujie Cai[3], Chen Yang[1]*

Spermidine, a ubiquitous polyamine, is known to be required for critical physiological functions in bacteria. Two principal pathways are known for spermidine biosynthesis, both of which involve aminopropylation of putrescine. Here, we identified a spermidine biosynthetic pathway via a previously unknown metabolite, carboxyaminopropylagmatine (CAPA), in a model cyanobacterium *Synechocystis* sp. PCC 6803 through an approach combining ^{13}C and ^{15}N tracers, metabolomics, and genetic and biochemical characterization. The CAPA pathway starts with reductive condensation of agmatine and L-aspartate-β-semialdehyde into CAPA by a previously unknown CAPA dehydrogenase, followed by decarboxylation of CAPA to form aminopropylagmatine, and ends with conversion of aminopropylagmatine to spermidine by an aminopropylagmatine ureohydrolase. Thus, the pathway does not involve putrescine and depends on L-aspartate-β-semialdehyde as the aminopropyl group donor. Genomic, biochemical, and metagenomic analyses showed that the CAPA-pathway genes are widespread in 15 different phyla of bacteria distributed in marine, freshwater, and other ecosystems.

INTRODUCTION

Polyamines are small organic polycations containing two or more amines. They are found in almost all cells of bacteria, archaea, and eukaryotes and play important roles in a variety of cellular processes, including gene regulation, cell proliferation and differentiation, and adaptation to various stresses (*1*–*5*). Polyamines are known to be necessary for critical physiological functions in bacteria, such as growth, biofilm formation, swarming, and production of siderophores (*6*).

The most ubiquitous polyamines in the three domains of life are the diamine putrescine and the triamine spermidine. There are two principal pathways for spermidine biosynthesis, which involve either direct or indirect aminopropylation of putrescine (*7*). The well characterized pathway, which is widely distributed in all three domains of life, involves the transfer of an aminopropyl group from decarboxylated *S*-adenosylmethionine (AdoMet) to putrescine by the aminopropyltransferase spermidine synthase (*8*–*10*). However, AdoMet decarboxylase and spermidine synthase are absent in many bacterial species (*11*–*13*). The other biosynthetic pathway of spermidine, which was proposed 40 years ago (*14*) and later characterized in a few bacterial species including plant pathogen *Agrobacterium tumefaciens* (*15*, *16*), depends on L-aspartate-β-semialdehyde (ASA) as the aminopropyl group donor. This pathway involves carboxyspermidine synthesized from putrescine by carboxyspermidine dehydrogenase (CASDH), which is then decarboxylated by carboxyspermidine decarboxylase (CASDC) to produce spermidine. Many bacterial genomes encode homologs of CASDH and CASDC (*13*); however, the polyamine biosynthetic pathway in most of these bacteria remains unclear. CASDH is the close homolog of carboxynorspermidine dehydrogenase (CANSDH), a key enzyme involved in norspermidine synthesis from 1,3-diaminopropane in *Vibrio* species (*17*–*19*). CASDH also shows sequence similarity to a large number of bacterial proteins that are annotated as saccharopine reductase (SR) or dehydrogenase in public databases (*13*, *19*). The exact function of these CASDH-like proteins remains largely to be elucidated. Improved understanding of bacterial polyamine biosynthesis may enable us to regulate the polyamine-related physiological functions in bacteria and to design the biocatalysts for production of polyamines (*20*, *21*).

In this study, we discovered a spermidine biosynthetic pathway via carboxyaminopropylagmatine (CAPA) in a model cyanobacterium *Synechocystis* sp. PCC 6803. Cyanobacteria are major primary producers of various ecosystems, and they colonize marine, freshwater, and terrestrial habitats (*22*–*24*). We used mass spectrometry (MS)–based metabolomics to quantitatively monitor the dynamic responses of cyanobacterial metabolism to sudden nutrient availability, which allowed us to identify two polyamines, i.e., CAPA and aminopropylagmatine (APA). By combining use of ^{13}C and ^{15}N tracers, metabolomics, and characterization of genetic mutants, we identified a spermidine biosynthetic pathway, which does not involve putrescine but includes a CASDH-like enzyme. Then, through detailed biochemical characterization, we identified a CAPA dehydrogenase (CAPADH) that catalyzes the reductive condensation of agmatine and ASA into CAPA, a CAPA decarboxylase (CAPADC) that decarboxylates CAPA to form APA, and an APA ureohydrolase (APAUH) that converts APA to spermidine. Last, on the basis of genomic, biochemical, and metagenome analyses, the phylogenetic distribution and ecological relevance of the CAPA pathway were studied.

[1]CAS-Key Laboratory of Synthetic Biology, CAS Center for Excellence in Molecular Plant Sciences, Shanghai Institute of Plant Physiology and Ecology, Chinese Academy of Sciences, Shanghai, China. [2]University of Chinese Academy of Sciences, Beijing, China. [3]The Key Laboratory of Industrial Biotechnology, Ministry of Education, School of Biotechnology, Jiangnan University, Jiangsu, China.
*Corresponding author. Email: niexiaoqun@cemps.ac.cn (X.N.); cyang@cemps.ac.cn (C.Y.)

RESULTS

Polyamine-related metabolites respond to nutrient upshifts

To obtain a comprehensive view of how cyanobacterial cells dynamically adjust their metabolism to adapt to environmental nutrient availability, we shifted a model cyanobacterium *Synechocystis* sp. PCC 6803 (hereafter denoted *Synechocystis*) from nitrogen-, phosphorous-, and sulfur-limited conditions to nutrient-replete condition and measured the metabolomic changes at various time points after each nutrient upshift. We found that, within 5 min after the nutrients were available, the intracellular concentrations of a large number of metabolites including biosynthetic pathway intermediates of amino acids and nucleotides increased substantially (fig. S1). These results were consistent with the rapid activation of biosynthesis of these precursor metabolites required for cell growth. Among the metabolites most severely affected by all the three nutrient upshifts, we observed a considerable and rapid increase in the concentrations of two unknown compounds with mass-to-charge ratio (*m*/*z*) of 188.187 and 232.177, respectively (Fig. 1, A and B).

The observed *m*/*z* of 188.187 and *m*/*z* of 232.177 were consistent with the chemical formula $C_8H_{22}N_5^+$ and $C_9H_{22}N_5O_2^+$, respectively. We performed molecular networking of tandem MS (MS/MS) spectra, which showed that *m*/*z* of 188.187 and 232.177 clustered with spermidine, acetylspermidine, agmatine, and arginine in a subnetwork (Fig. 1C). The MS/MS spectra of *m*/*z* of 188.187 and 232.177 and agmatine shared the neutral loss of guanidine (Δ59.048 Da) and a prominent daughter ion of *m*/*z* of 114.103, corresponding to deaminated agmatine (fig. S2). Fragmentation of *m*/*z* of 188.187 showed that the daughter ion of *m*/*z* of 114.103 resulted from the loss of 74.084 Da ($C_3H_{10}N_2$), which was revealed as a 1,3-diaminopropane moiety by the MS/MS spectrum of spermidine. Thus, we tentatively assigned the metabolite with *m*/*z* of 188.187 to APA and the metabolite with *m*/*z* of 232.177 to CAPA, a previously unidentified polyamine (Fig. 1D). The proposed structures were confirmed by nuclear magnetic resonance (NMR) analysis of the purified compounds (figs. S3 and S4).

Identification of a spermidine biosynthetic pathway via CAPA

To investigate the biosynthetic origin of the two polyamines, CAPA and APA, we conducted ^{13}C- and ^{15}N-labeling experiment by using uniformly (*U*) labeled [*U*-^{13}C, *U*-^{15}N]arginine as a tracer (Fig. 2A). *Synechocystis* cells were exponentially growing in medium containing the stable isotope tracer, and, then, the labeling of individual metabolites was analyzed by liquid chromatography (LC)–MS/MS. [*U*-^{13}C, *U*-^{15}N]agmatine was detected (Fig. 2B), which was generated from [*U*-^{13}C, *U*-^{15}N]arginine through the reaction catalyzed by arginine decarboxylase (ADC) (*25*, *26*). We found that the ^{13}C and ^{15}N labels were incorporated into the agmatine moiety of CAPA and APA and the 1,4-diaminobutane moiety of spermidine (Fig. 2B and fig. S5). As carboxyspermidine and carboxynorspermidine are known as intermediates of ASA-dependent biosynthetic

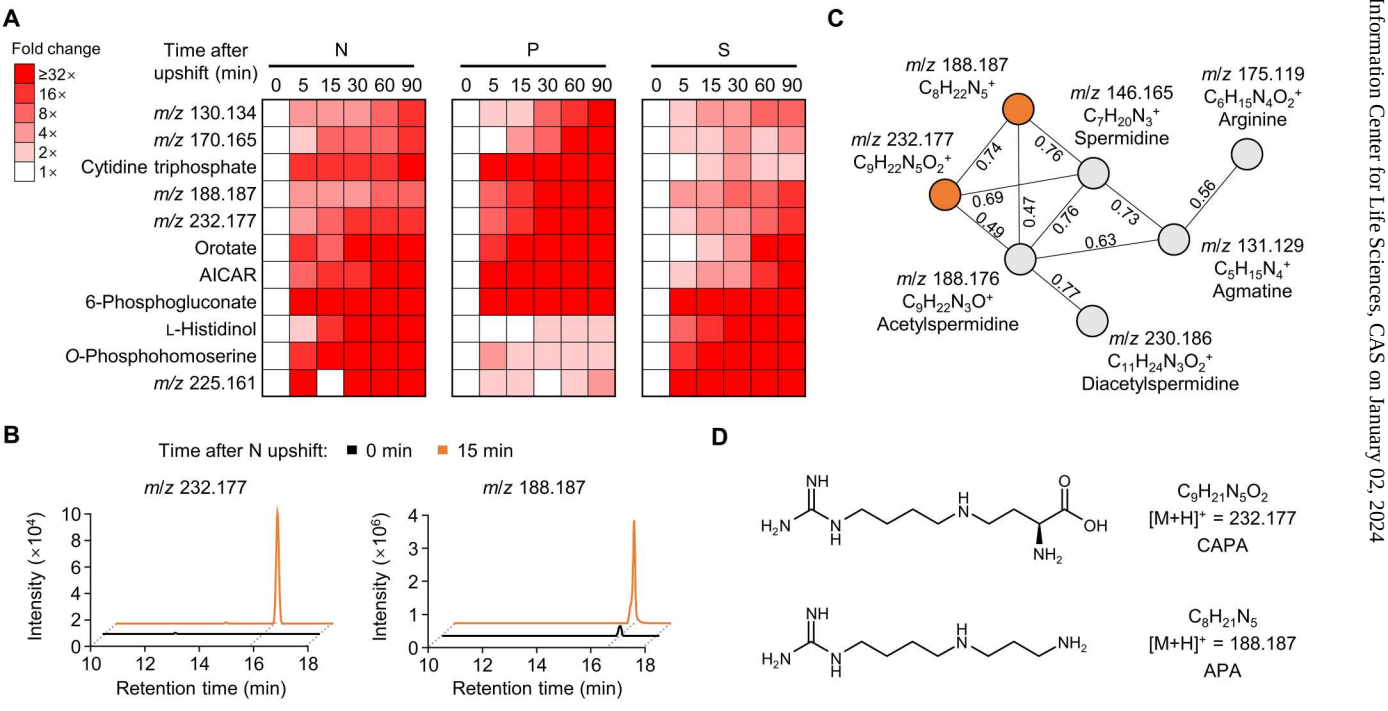

Fig. 1. Polyamine-related metabolites respond to nutrient upshifts. (**A**) Metabolomic changes in *Synechocystis* induced by nitrate (N), phosphate (P), and sulfate (S) upshifts. Data for the metabolites with concentrations significantly and rapidly increased after all the three nutrient upshifts are shown in heatmap format. Metabolite concentrations of two cell cultures were averaged and normalized to those of nutrient-starved cells (time zero), and the resulting fold changes were $\log_2$-transformed. AICAR, 5-aminoimidazole carboxamide ribonucleotide. (**B**) Liquid chromatography (LC)–MS extracted ion chromatograms (EICs) for *m*/*z* of 232.177 and 188.187 from exacts of cells collected before (0 min) and 15 min after nitrate upshift. (**C**) MS/MS subnetwork containing *m*/*z* of 232.177 and 188.187 and polyamines. The similarity scores between the MS/MS spectra of metabolites (nodes) are shown. (**D**) Structures of the two metabolites with *m*/*z* of 232.177 and 188.187, respectively, as determined on the basis of tandem MS (MS/MS) fragmentation and nuclear magnetic resonance (NMR) spectra.

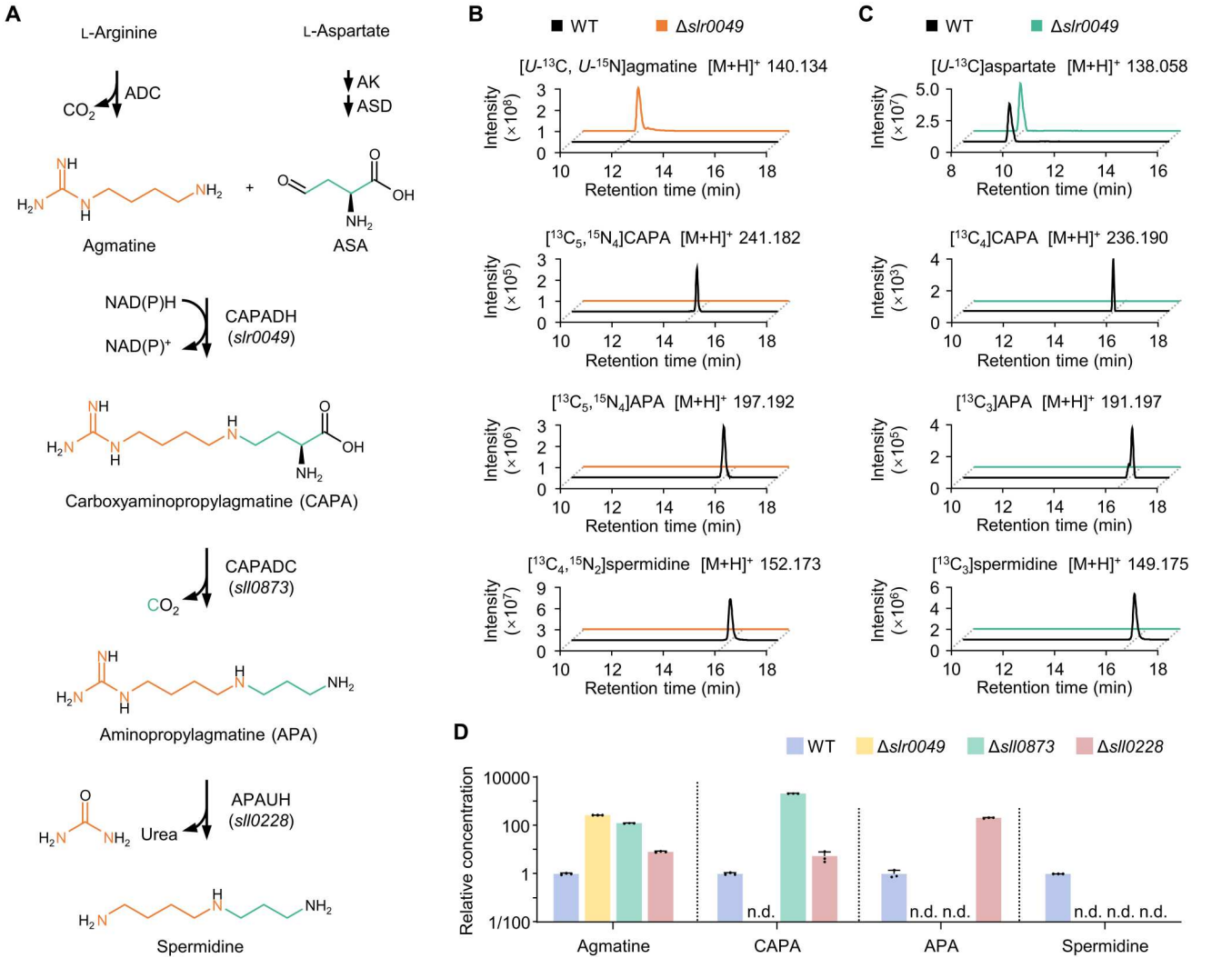

Fig. 2. Identification of a spermidine biosynthetic pathway. (**A**) Schematic of [*U*-^{13}C, *U*-^{15}N]arginine– and [*U*-^{13}C]asparagine–derived labeling through the proposed spermidine biosynthetic pathway. Labeled carbon and nitrogen from [*U*-^{13}C, *U*-^{15}N]arginine are shown in orange, and labeled carbon from [*U*-^{13}C]asparagine is shown in green. ADC, arginine decarboxylase; AK, aspartokinase; ASD, L-ASA dehydrogenase. (**B** and **C**) LC-MS EICs of spermidine-biosynthetic-pathway intermediates in the wild-type and *slr0049*-deleted mutant growing in [*U*-^{13}C, *U*-^{15}N]arginine (B) and [*U*-^{13}C]asparagine (C) media. Data shown are representative of $n = 3$ independent experiments that yielded identical results. (**D**) Relative metabolite concentrations in the gene deletion mutants Δ*slr0049*, Δ*sll0873*, and Δ*sll0228* compared to the wild type (WT). Data shown are means ± SD ($n = 3$ independent experiments). n.d., not detectable.

pathways of spermidine and norspermidine, respectively, we tested whether ASA is involved in biosynthesis of CAPA and APA. We incubated *Synechocystis* cells with [*U*-^{13}C]asparagine, which generated [*U*-^{13}C]aspartate through asparaginase activity (Fig. 2C). Although ASA could not be detected by LC-MS, owing to its lability, [*U*-^{13}C]ASA could be synthesized from the labeled aspartate (Fig. 2A). We observed the incorporation of ^{13}C into the carboxyaminopropyl group of CAPA and the aminopropyl group of APA and spermidine (Fig. 2C and fig. S6). These results suggest that both agmatine and ASA are precursors for biosynthesis of CAPA, APA, and spermidine.

To identify the genes responsible for biosynthesis of CAPA and APA in *Synechocystis*, we deleted the genes *slr0049*, *sll0873*, and *sll0228* (fig. S7), which have been proposed to be involved in spermidine biosynthesis (*27*–*29*). Slr0049 and Sll0873 are annotated as saccharopine dehydrogenase family protein and carboxynorspermidine decarboxylase (CANSDC), respectively, and Sll0228 has been proposed to be an arginase or agmatine ureohydrolase. We compared the intracellular metabolite concentrations between the gene-deletion mutants and wild-type strain. Deletion of any of the three genes led to substantial accumulation of agmatine and complete depletion of spermidine (Fig. 2D and fig. S8A). Specifically, the *slr0049*-knockout mutant, compared with the wild type, exhibited 270-fold higher level of agmatine and undetectable CAPA and APA. The lack of CAPA, APA, and spermidine in this mutant was confirmed by the ^{13}C- and ^{15}N-labeling experiments (Fig. 2, B and C). In the *sll0873*-deleted mutant, the CAPA concentration was over 2100-fold higher than that in the wild type, whereas APA was not detectable (Fig. 2D). Meanwhile, a 200-fold increase in the APA level was observed in the *sll0228*-knockout mutant

compared to the wild type. These results suggest that Slr0049, Sll0873, and Sll0228 are required to convert agmatine to CAPA, CAPA to APA, and APA to spermidine, respectively.

Complementation of the individual gene-deletion mutants by expressing the respective genes fully restored the spermidine biosynthesis (fig. S8A). Thus, the genes *slr0049*, *sll0873*, and *sll0228* are essential for the spermidine biosynthesis in *Synechocystis*. We found that, although Slr0049 shows sequence similarity to CASDH, which catalyzes the condensation of putrescine and ASA into carboxyspermidine, the *slr0049*-knockout mutant showed a remarkable decrease in putrescine concentration compared with the wild type (fig. S8B). Carboxyspermidine was not detectable in both the mutant and wild type (fig. S8C). Moreover, the extent of putrescine labeling derived from [*U*-^{13}C, *U*-^{15}N]arginine was substantially lower than that of spermidine in the wild type (fig. S5B). These results indicate that putrescine is not a precursor for spermidine biosynthesis but likely a product from spermidine oxidation, which is supported by a recent report on polyamine oxidase from *Synechocystis* (*30*). Therefore, on the basis of ^{13}C- and ^{15}N-labeling experiments, detailed metabolite analysis, and characterization of genetic mutants, we propose a putrescine-independent biosynthetic pathway of spermidine via CAPA and APA in *Synechocystis*.

CAPADH catalyzes reductive condensation of agmatine and ASA into CAPA

To test whether Slr0049, Sll0873, and Sll0228 catalyze the proposed reactions for spermidine biosynthesis, we reconstituted the CAPA pathway in vitro using purified recombinant enzymes from *Synechocystis* (fig. S7B). Slr0049, Sll0873, and Sll0228 were added to the assay mixture containing agmatine, homoserine, nicotinamide adenine dinucleotide phosphate ($NADP^+$), and homoserine dehydrogenase that converts homoserine and $NADP^+$ to ASA and reduced form of $NADP^+$ (NADPH). Spermidine could be detected only in the presence of all the three *Synechocystis* enzymes (Fig. 3A). Complete conversion of agmatine to spermidine was achieved after overnight incubation of the reaction mixture. To confirm that Slr0049 synthesizes CAPA from agmatine and ASA, we performed biochemical assays using chemically synthesized ASA. Incubation of Slr0049 with agmatine, NADPH, and ASA led to the formation of CAPA with MS/MS spectrum and retention time identical to those of CAPA (*m*/*z* of 232.177) in extracts of *Synechocystis* cells (Fig. 3B and fig. S9, A and B). Formation of CAPA by the reaction was also validated by NMR. In contrast, CAPA was not measurable in the absence of NADPH (fig. S9A). Therefore, we propose that Slr0049 catalyzes the NADPH-dependent condensation of agmatine and ASA into CAPA.

Slr0049 is a CAPADH that has not been identified previously. Kinetic characterization of this enzyme toward agmatine showed a turnover number (k_{cat}) of 2.57 s^{-1} and Michaelis constant (K_m) of 10 μM (Table 1 and fig. S9C), which is within the physiological concentration range of agmatine (2 to 500 μM) in *Synechocystis*. Although the enzyme activity toward putrescine and 1,3-diaminopropane was detectable (fig. S9D), the k_{cat}/K_m values are three to four orders of magnitude lower than that for agmatine, and the high K_m values rule them out as feasible physiological substrates (Table 1 and fig. S9C). In addition, the CAPADH is incapable of accepting cadaverine or spermidine (fig. S9D). Thus, the CAPADH is specific to agmatine. The K_m value for NADPH is 50 times lower than that for NADH (Table 1), indicating that NADPH is the preferred cofactor for CAPADH. The preference for NADPH has also been observed for two related enzymes: CANSDH (*19*) and SR (*31*). SR, also called saccharopine dehydrogenase (L-glutamate-forming), is a distant homolog of CAPADH (~19% of sequence identity) and catalyzes the reductive condensation of glutamate and α-aminoadipate-δ-semialdehyde into saccharopine.

We next performed homology modeling and docking to gain an insight into the CAPADH reaction. The reference used for homology modeling was the structure of NADPH-complexed SPD_0812 from *Streptococcus pneumoniae* [Protein Data Bank (PDB), 4RL6], which shares 56% sequence identity with *Synechocystis* CAPADH.

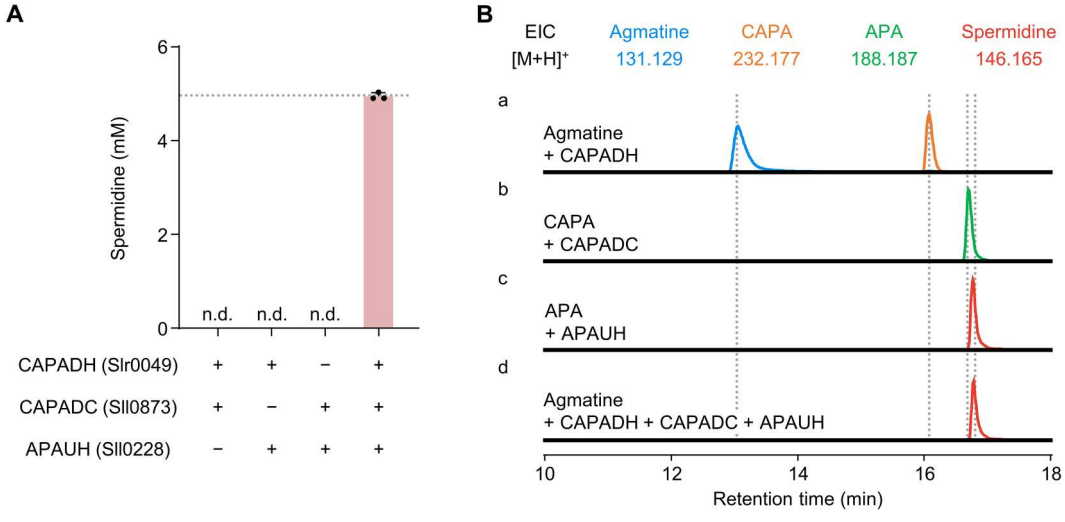

Fig. 3. Characterization of the CAPA-pathway enzymes. (**A**) In vitro reconstitution of spermidine synthesis via the CAPA pathway. The purified recombinant enzymes CAPADH, CAPADC, and APAUH were added to the assay mixture containing agmatine, homoserine, $NADP^+$, and homoserine dehydrogenase. The gray dotted line indicates complete conversion of agmatine (5 mM). Data shown are means ± SD (n = 3 independent experiments). (**B**) LC-MS EICs of products from incubation of (a) CAPADH with agmatine, ASA, and NADPH; (b) CAPADC with CAPA; (c) APAUH with APA; and (d) CAPADH, CAPADC, and APAUH with agmatine, homoserine, $NADP^+$, and homoserine dehydrogenase. Data shown are representative of n = 3 independent experiments that yielded identical results.

Table 1. Kinetic parameters of the three enzymes of CAPA pathway. Data are means ± SD, as determined from nonlinear fits of three independent experimental data with GraphPad Prism 9. Michaelis-Menten fits of enzyme kinetics for CAPADH, CAPADC, and APAUH are provided in figs. S9, S11, and S12, respectively. For CAPADH, kinetics for agmatine, putrescine, and 1,3-diaminopropane were measured with 1.25 mM ASA and 0.25 mM NADPH; kinetics for NADPH and NADH were measured with 1.25 mM ASA and 5 mM agmatine.

Enzyme	Substrate	k_{cat} (s^{-1})	K_m (mM)	k_{cat}/K_m (M^{-1} s^{-1})
CAPADH	Agmatine	2.57 ± 0.05	0.01 ± 0.001	2.57×10^5
	Putrescine	0.32 ± 0.01	6.34 ± 0.27	5.10×10^1
	1,3-Diaminopropane	0.07 ± 0.01	2.67 ± 0.48	2.80×10^1
	NADPH	2.43 ± 0.04	0.01 ± 0.001	2.43×10^5
	NADH	–	0.58 ± 0.07	–
CAPADC	CAPA	2.36 ± 0.09	0.21 ± 0.03	1.10×10^4
APAUH	APA	70.80 ± 2.45	1.78 ± 0.14	4.00×10^4

Although SPD_0812 was annotated as a saccharopine dehydrogenase, it was proposed as a CAPADH based on our enzymatic analysis of the purified protein (see below). The structure of SPD_0812 is similar to two recently published structures of CASDH-like enzymes from *Helicobacter pylori* (*32*) and *Bacteroides fragilis* (*33*) and is a homodimer with each monomer consisting of a NADPH-binding domain with a modified Rossman fold and a C-terminal substrate-binding domain. We then developed a docking model of *Synechocystis* CAPADH with CAPA by referring to the structure of saccharopine- and NADPH-complexed SR from *Magnaporthe grisea* (PDB, 1E5Q) (*34*). On the basis of the orientation of the saccharopine, the CAPA molecule was docked into the active site of CAPADH (fig. S10A). Within this structure, the C4 carbon atom of CAPA is located in the vicinity of the NADPH nicotinamide ring (Fig. 4A). CAPA is held in place by several hydrogen bonds and π-cation interaction. The guanidine group of CAPA forms hydrogen bonds to N104, E106, and E228. The positively charged guanidine group is involved in cation-π interaction with the aromatic ring of F113. The amino group of CAPA is recognized by the side chain of D165. The carboxyl group of CAPA interacts with the N^{τ} atom of the side chain of H227 and the carboxamide moiety of the nicotinamide ring. Superimposition of the structures of SR with CAPADH revealed that the Rossman fold structures bind the coenzymes in a similar active site (fig. S10A). However, their substrates were not well superimposed. Consistently, most of the residues that are responsible for substrate binding in SR are not conserved in CAPADH except D126. This residue is conserved as D139 in CAPADH (fig. S10A). In addition, E187, T342, and T343 were observed to be close to the C4 of CAPA or the nicotinamide ring in the active site (Fig. 4A). On the basis of the reaction mechanism of SR (*34*, *35*), we speculate that the CAPADH reaction involves a nucleophilic attack by the amino group of agmatine on the aldehyde carbonyl of ASA, followed by elimination of water from a carbinolamine intermediate and reduction of the generated Schiff base intermediate by NADPH to yield CAPA.

To substantiate the involvement of the abovementioned amino acid residues in substrate binding or catalysis, we constructed E106A, D139A, D165A, E187A, H227A, E228A, T342A, and T343A variants. All these variants showed significantly lower activity than the wild-type enzyme (Fig. 4B). In particular, the mutations of D165, H227, and E228 completely abolished the enzyme activity. The enzyme variants N104A, N104Q, F113A, and F113W were also constructed and kinetically analyzed. Compared to the wild-type enzyme, the K_m values of the four variants for agmatine increase 7- to 150-fold, whereas their catalytic activities are similar or even increased (fig. S10B), which supports a role of N104 and F113 in the substrate binding.

CAPADH is closely related to CASDH and CANSDH with approximately 40 and 42% sequence identities, respectively. In addition, CAPADH shares sequence similarity to SR, lysine 6-dehydrogenase (LysDH), and homospermidine synthase (HSS). All these enzymes are members of the saccharopine dehydrogenase family (Pfam, PF16653). The three amino acids N104, F113, and E228 are only conserved in CAPADH orthologs, providing a signature sequence for this enzyme group (fig. S10C). They are replaced by I113, W126, and D241 in *A. tumefaciens* CASDH and V112, E125, and D240 in *Vibrio cholerae* CANSDH, respectively. Meanwhile, E106, D139, D165, E187, H227, T342, and T343 in CAPADH are conserved in CASDH and/or CANSDH. Most of these residues are variable in SR, LysDH, and HSS. Phylogenetic analysis revealed that CAPADH and its orthologs are clustered as a separate group from CASDH and CANSDH and form a distinct clade within the saccharopine dehydrogenase family (Fig. 4C and fig. S10D).

CAPADC decarboxylates CAPA to form APA

To determine whether Sll0873 catalyzes the decarboxylation of CAPA, we performed biochemical assays using CAPA, which was enzymatically produced and then isolated from the reaction mixture. Incubation of the purified Sll0873 with CAPA and pyridoxal 5′-phosphate (PLP) yielded NMR-validated APA with MS/MS spectrum and retention time identical to those of APA (*m*/*z* of 188.187) in extracts of *Synechocystis* cells (Fig. 3B and fig. S11, A and B). In addition, carbon dioxide was detected in the reaction products through an enzymatic assay (fig. S11C). Thus, through genetic and biochemical characterization, we propose that Sll0873 is a CAPADC, which has not been identified previously.

The k_{cat} of the CAPADC is 2.36 s^{-1}, which is comparable to that of the CAPADH (Table 1 and fig. S11D). The K_m value for CAPA is 0.21 mM. To assess the enzyme activity toward carboxyspermidine and carboxynorspermidine, the CAPADC was incubated with the reaction products of *A. tumefaciens* CASDH and *V. cholerae* CANSDH, respectively. Significant amounts of spermidine and norspermidine were detected in the respective assay mixtures, indicating that carboxyspermidine and carboxynorspermidine were decarboxylated by CAPADC with an activity comparable to those of *A. tumefaciens* CASDC and *V. cholerae* CANSDC (fig. S11E). Similarly, CASDC and CANSDC have been shown to accept both carboxyspermidine and carboxynorspermidine (*19*, *36*). However,

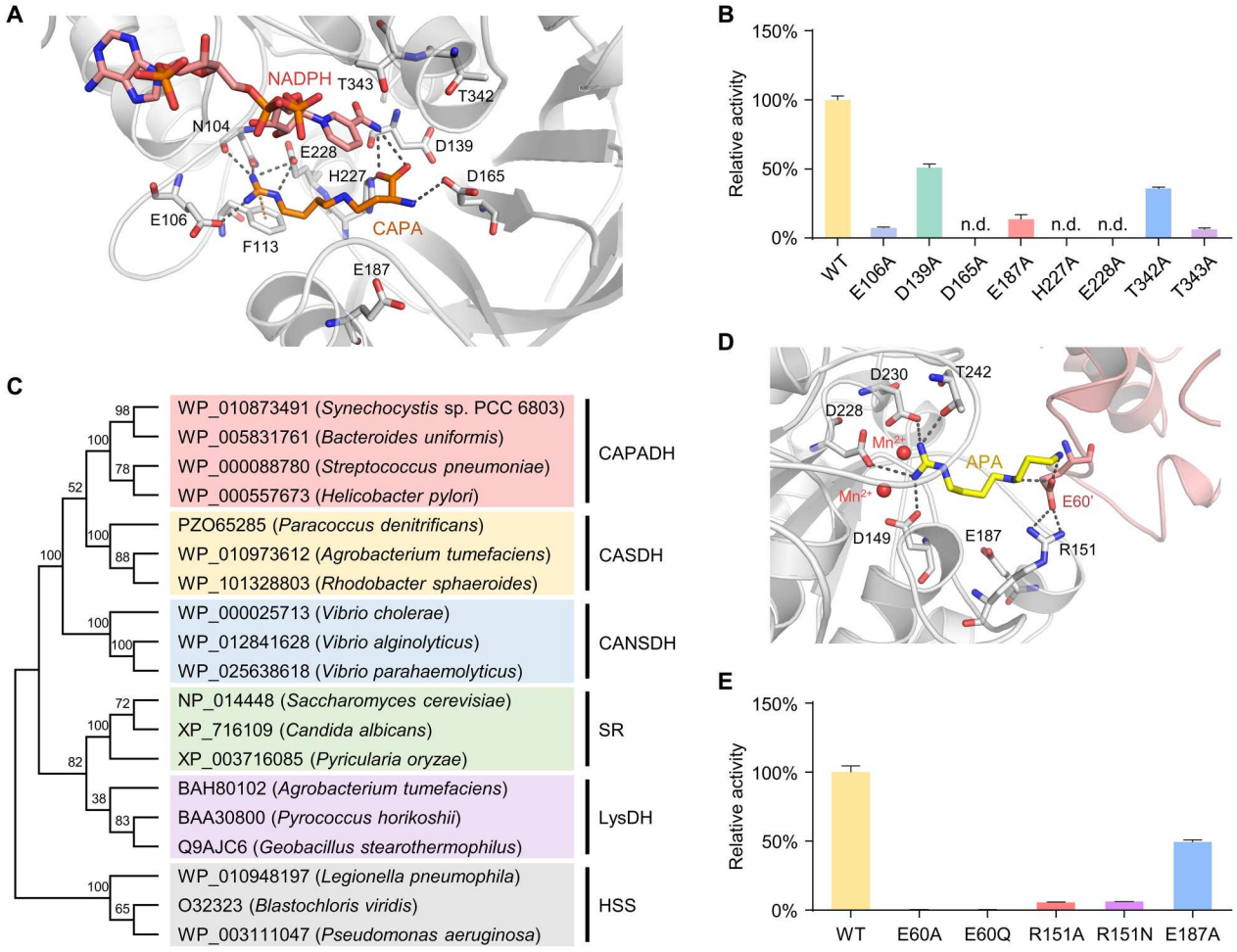

Fig. 4. Docking, mutagenesis, and phylogenetic analysis of the CAPA-pathway enzymes. (**A**) Active site in the docking model of NADPH (pink)–complexed CAPADH with CAPA (orange). Hydrogen bonds are depicted as gray dotted lines and π-cation interaction as orange dotted line. (**B**) Relative activities of CAPADH mutants compared to the wild-type enzyme. Data shown are means ± SD (n = 3 independent experiments). (**C**) Neighbor-joining tree of CAPADH and its orthologs and other proteins from the saccharopine dehydrogenase family. Sequence similarity network (SSN) of 31,294 sequences from this family is shown in fig. S10D. (**D**) Active site in the docking model of Mn^{2+} (magenta)–bound APAUH with APA (yellow). Hydrogen bonds are depicted as gray dotted lines. (**E**) Relative activities of APAUH mutants compared to the wild-type enzyme. Data shown are means ± SD (n = 3 independent experiments).

CAPADC is incapable of decarboxylating ornithine, arginine, lysine, and *meso*-diaminopimelate (fig. S11F).

CAPADC is closely related to CASDC and CANSDC and exhibits low sequence identity to ornithine, arginine, lysine, and *meso*-diaminopimelate decarboxylases. All these enzymes are PLP-dependent decarboxylases with the alanine racemase (AR) fold (*36*). We developed a docking model of CAPADC with CAPA based on the structure of PLP- and norspermidine-complexed CANSDC or CASDC from *Campylobacter jejuni* (PDB, 3 N29) (*36*), which shares 39% sequence identity with Sll0873. The active site residues E183, S250, D287, Y293, D342, and H345 were proposed to interact with the CAPA molecule (fig. S11G). Although S250 and H345 are less conserved, E183, D287, Y293, and D342 are completely conserved among CAPADC, CANSDC, and CASDC (fig. S11H). These residues distinguish the active site of CAPADC, CANSDC, and CASDC from other AR-fold decarboxylases.

APAUH converts APA to spermidine and urea

To confirm that Sll0228 catalyzes the conversion of APA to spermidine, we performed biochemical assays using APA that was isolated from enzymatic reaction products. Incubation of the purified Sll0228 with APA resulted in the formation of spermidine, which was identified by high-performance LC (HPLC) and further validated by LC-MS (Fig. 3B and fig. S12, A and B). Urea was detected in the reaction products through both a colorimetric assay and gas chromatography (GC)–MS (fig. S12C). Complete conversion of APA to spermidine and urea was achieved after 1 hour of incubation of the reaction mixture (fig. S12, A and B). Thus, through genetic and biochemical characterization, we propose that Sll0228 is an APAUH.

The APAUH activity has only been described in the extreme thermophile *Thermus thermophilus* (*37*) and hyperthermophilic archaeon *Thermococcus kodakarensis* (*38*). In both organisms, APA is synthesized from agmatine by an aminopropyltransferase using decarboxylated AdoMet as the aminopropyl group donor (*39*). Like

arginase and agmatine ureohydrolase, the purified APAUH contains 1.34 Mn^{2+} per subunit (fig. S12D). Kinetic characterization of *Synechocystis* APAUH toward APA shows a k_{cat} of 70.8 s^{-1} and K_m of 1.78 mM (Table 1 and fig. S12E). Thus, among the three enzymes of CAPA pathway, APAUH has the highest catalytic activity. Putrescine was not detectable in the assay mixture containing the APAUH and agmatine (fig. S12F). The APAUH is highly specific to APA and incapable of releasing measurable urea from CAPA, agmatine, arginine, guanidine, guanidinobutyrate, and guanidinopropionate (fig. S12G).

We computed a homology model of APAUH based on the structure of a manganese ions-bound ureohydrolase from *Thermoplasma volcanium* (PDB, 3PZL), which shares 32% sequence identity with Sll0228 and is proposed as an APAUH based on our biochemical analysis (fig. S13A). The APA molecule was then docked into the active site of APAUH model by referring to the structure of Mn^{2+}- and arginine-complexed arginase from *Bacillus caldovelox* (PDB, 3CEV) (fig. S13C) (*40*). Within this structure, the guanidine group of APA is adjacent to the dimanganese center (Fig. 4D). The Mn^{2+}-coordinating residues D149, D228, and D230 as well as T242 forms hydrogen bonds to the guanidine group. The 1,3-diaminopropane moiety of APA interacts with E60 from a neighboring subunit. This residue forms a hydrogen bond to R151. The amino acids D149, D228, D230, and T242 are conserved among the ureohydrolase superfamily proteins, whereas E60 and R151 are only conserved in the APAUH orthologs (fig. S13B). Consistently, the constructed E60A, E60Q, R151A, and R151N variants retained only 1 to 6% of the wild-type activity (Fig. 4E). In addition, E187 in APAUH corresponds to E181 in arginase (fig. S13C), which interacts with the amino group of arginine (*40*). The E187A substitution also significantly decreased the enzymatic activity (Fig. 4E). Phylogenetic analysis revealed that APAUH and its orthologs are clustered as a separate group from arginase and agmatine ureohydrolase and form a distinct clade within the ureohydrolase superfamily (fig. S13D).

The CAPA pathway is widely distributed in bacteria

On the basis of the in vivo and in vitro experimental results described above, a spermidine biosynthetic pathway via CAPA was identified in *Synechocystis*. We next studied the phylogenetic distribution of the CAPA pathway. The pathway genes were searched against the reference and representative bacterial genomes in the National Center for Biotechnology Information (NCBI) RefSeq database. As a result, 2077 of the 16,546 bacterial species were found to harbor both the CAPADH- and CAPADC-encoded genes (table S1), which are often neighboring genes on the chromosome (Fig. 5). These species belong to 15 different bacterial phyla including Cyanobacteria, Bacteroidetes, Proteobacteria, Spirochaetes, Fibrobacteres, Firmicutes, Planctomycetes, Deinococcus-Thermus, Deferribacteres, Verrucomicrobia, Kiritimatiellaeota, Fusobacteria, Chrysiogenetes, Lentisphaerae, and Actinobacteria (fig. S14A). Most of these species also encode ADC in their genomes (Fig. 5), enabling them to decarboxylate arginine to agmatine for subsequent spermidine synthesis through the CAPA pathway. Notably, the APAUH orthologs are present in 44% of the species with the CAPADH and CAPADC, whereas the rest of the species have the genes encoding agmatine deiminase/iminohydrolase- and *N*-carbamoylputrescine amidohydrolase-like enzymes (*41*, *42*). Both genes are clustered with the CAPADH- and CAPADC-encoded genes in some genomes (Fig. 5); thus, it is tempting to speculate that APA may be converted to spermidine by the concerted action of APA deiminase/iminohydrolase and *N*-carbamoylspermidine amidohydrolase in these species (e.g., *S. pneumoniae*).

The CAPA-pathway genes are widespread among Proteobacteria, Firmicutes, and Bacteroidetes (Fig. 5 and fig. S14A). A large proportion of delta- and epsilonproteobacterial genomes encode CAPADH and CAPADC (Fig. 5). In particular, in the Epsilonproteobacteria, the CAPA pathway is probably a predominant pathway for spermidine biosynthesis. However, the CAPADH orthologs are absent in over 1000 betaproteobacterial species analyzed. In some Firmicutes species with the CAPA pathway, the genes encoding AdoMet decarboxylase and spermidine synthase are also present (Fig. 5), suggesting the existence of both pathways for spermidine biosynthesis (*43*). The CAPA-pathway genes were also found in a majority of species in several less sequenced phyla such as Deinococcus-Thermus. Although the CAPA pathway was identified in *Synechocystis*, the CAPADH orthologs were detected in only 10 of the 184 cyanobacterial species. In addition, the CAPA-pathway genes are rare in Actinobacteria and Planctomycetes. To support the proposed distribution of the CAPA pathway, we performed biochemical characterization of CAPADH orthologs from seven representative bacterial species. They are the deltaproteobacterial species *Desulfovibrio vulgaris* and *Geobacter sulfurreducens*, the epsilonproteobacterium *H. pylori*, the Firmicutes species *S. pneumoniae*, the Bacteroidetes species *Bacteroides uniformis*, the Deinococcus-Thermus species *Deinococcus radiodurans*, and the filamentous cyanobacterium *Leptolyngbya* sp. BL0902. We observed the production of CAPA from incubation of each of the seven purified recombinant enzymes with agmatine, ASA, and NADPH (fig. S14, B and C). Similar to *Synechocystis* CAPADH, these enzymes showed much lower activities toward putrescine and 1,3-diaminopropane than the activity for agmatine (fig. S14D). Thus, these enzymes are functional CAPADH probably involved in spermidine biosynthesis in the species from diverse bacterial phyla.

DISCUSSION

Spermidine is a ubiquitous polyamine in bacteria. In this study, by combining use of ^{13}C and ^{15}N tracers, metabolomics, and genetic and biochemical characterization, we identified a spermidine biosynthetic pathway via a previously unknown metabolite, CAPA, in *Synechocystis*. The CAPA pathway involves two previously unkown reactions, which are NADPH-dependent condensation of agmatine and ASA into CAPA by a CAPADH and decarboxylation of CAPA to APA by a CAPADC. Spermidine is then synthesized from APA through a previously unappreciated ureohydrolase APAUH. The CAPA pathway does not involve putrescine and uses ASA rather than decarboxylated AdoMet as the aminopropyl group donor; thus, it is different from the known biosynthetic pathways of spermidine. Comparing with the spermidine synthase pathway that requires the synthesis of energetically costly AdoMet and the salvage of the coproduct methylthioadenosine (*44*), the CAPA pathway needs only less adenosine 5′-triphosphate for synthesis of ASA. The individual enzymes of the CAPA pathway share sequence similarity to those of the carboxyspermidine pathway and the carboxynorspermidine pathway, indicating that the three pathways may have evolved independently from a common ancestor (*43*, *45*). All the intermediates in the CAPA pathway, i.e., agmatine,

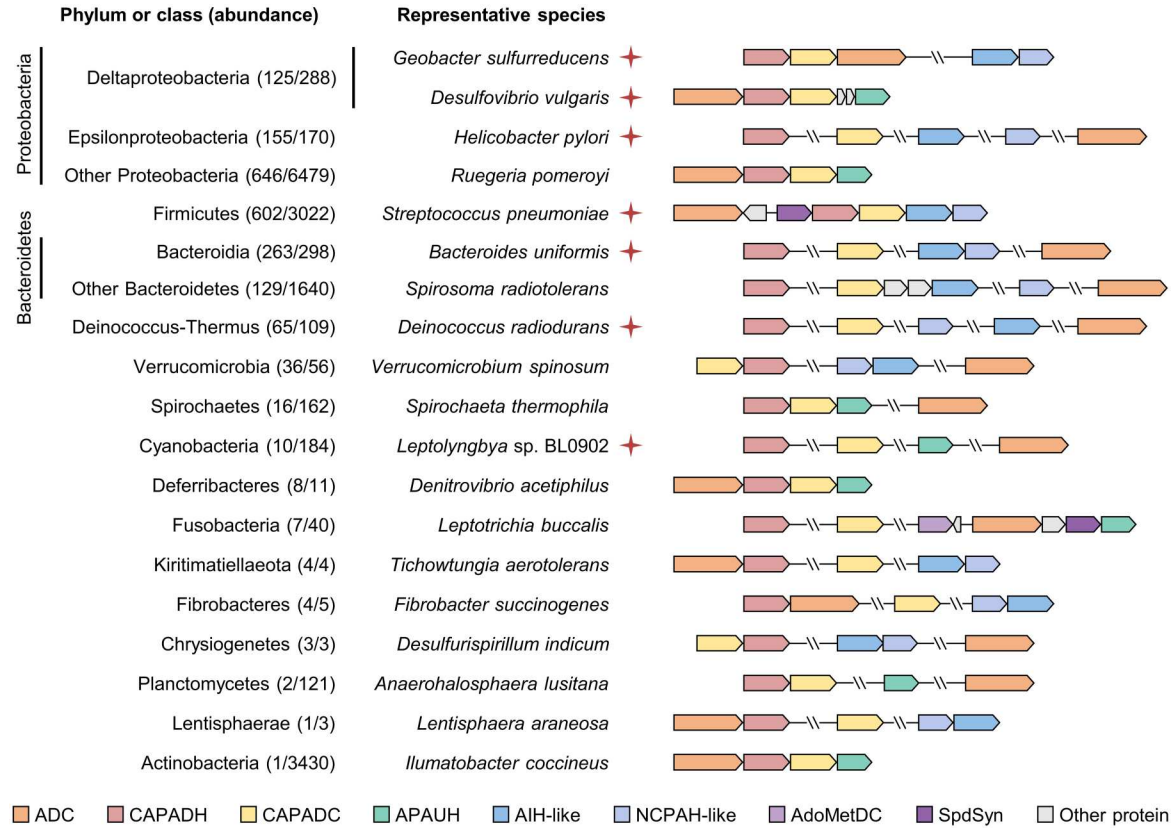

Fig. 5. Distribution of the CAPA pathway in bacteria. The CAPA-pathway genes and related genes are shown by arrows. The number of bacterial species with the CAPA-pathway genes and the total number of bacterial species analyzed in individual phyla or classes are indicated in parentheses. The species with CAPADH that were characterized in this study are indicated by red asterisks.

CAPA, and APA, bear the guanidine group that can form hydrogen bonds and cation-π interaction with the pathway enzymes. This ability of the guanidine group, which is widely exploited in synthetic medicinal chemistry (*46*, *47*), may contribute to the high affinity of CAPADH and CAPADC toward their substrates.

Unlike eukaryotes and archaea that absolutely need spermidine in deoxyhypusine synthase-catalyzed reaction for hypusine modification of the translation factor, initiation factor 5A (IF5A), the polyamine function is diverse and poorly understood in bacteria (*6*). We found that the CAPA pathway was rapidly and significantly activated in cyanobacterial cells in response to sudden availability of essential nutrients, indicating a high priority of activation of spermidine biosynthesis for restoration of cellular growth and metabolism. A previous study has shown that deficiency in CAPADH or CAPADC had no significant effect on cell growth but reduced the survivability of *Synechocystis* under chill-light stress (*27*). As homospermidine, norspermidine, and aminopropylcadaverine that could serve as a replacement for spermidine (*15*, *48*, *49*) were absent in these *Synechocystis* mutants, we speculate that high levels of agmatine, CAPA, and APA could replace the function of spermidine in cell growth. We observed that knockout of ADC-encoded genes abolished the growth of the resulting strain and the cell growth was restored by addition of agmatine to the medium. However, the role of spermidine in survival of cyanobacterial cells under stress conditions could not be fully replaced by the CAPA-pathway intermediates. For other bacteria harboring the CAPA-pathway genes, diverse requirements for spermidine in cell growth have been reported (*50*–*52*). Further studies are required to understand the molecular function of spermidine and CAPA-pathway intermediates in bacteria, which could be aided by the metabolomic approach described here.

The CAPA-pathway genes are found in many bacteria from diverse phyla. These bacterial strains were isolated from a wide variety of ecosystems, including animal digestive system, soil, marine, freshwater, sediments, and engineered habitats (fig. S15A and table S1). To further understand the ecological importance of the CAPA pathway, we analyzed 497 metagenomes collected from diverse habitats for the presence of CAPADH as representative enzyme of the pathway. CAPADH is ubiquitously present in 254 human gut metagenomes, 199 marine metagenomes, and 44 freshwater metagenomes (fig. S15B). As the CAPA-pathway genes are pervasive in Bacteroidetes and Firmicutes, the two dominant bacterial phyla within the human large intestine (figs. S14A and S15C), the bacteria harboring this pathway accounts for about 47% (median) of the total bacterial abundance in the human gut metagenomes. In marine and freshwater environments, the CAPA-pathway genes are mainly found in Proteobacteria (fig. S15C). Because of the low energy cost and unnecessity for salvage, the CAPA pathway, compared to the spermidine synthase pathway, may confer a growth advantage to bacterial cells in energy-limited environments. This may have contributed to the prevalence of the

CAPA pathway in gut Bacteroidetes and Firmicutes as well as marine and freshwater Proteobacteria.

MATERIALS AND METHODS

Strains and culture conditions

Synechocystis sp. PCC 6803 strains were routinely grown under continuous white light (~75 μmol quanta m^{-2} s^{-1}) at 30°C in BG-11 medium (*53*), which contains (per liter) 1.5 g of $NaNO_3$, 40 mg of $K_2HPO_4{\cdot}3H_2O$, 75 mg of $MgSO_4{\cdot}7H_2O$, 36 mg of $CaCl_2{\cdot}2H_2O$, 20 mg of Na_2CO_3, 6 mg of citric acid, 6 mg of ferric ammonium citrate, 1 mg of EDTA-Na_2, 2.86 mg of H_3BO_3, 1.55 mg of $MnSO_4{\cdot}H_2O$, 0.22 mg of $ZnSO_4{\cdot}7H_2O$, 0.04 mg of $Na_2MoO_4{\cdot}2H_2O$, 0.08 mg of $CuSO_4{\cdot}5H_2O$, and 0.05 mg of $Co(NO_3)_2{\cdot}6H_2O$. Nitrate was excluded in the nitrogen-deficient medium, and the phosphorous-deficient medium lacked phosphate. The sulfur-deficient medium was prepared by replacing $MgSO_4$, $MnSO_4$, $ZnSO_4$, and $CuSO_4$ with 0.3 mM $MgCl_2$, 9 μM $MnCl_2$, 0.8 μM $ZnCl_2$, and 0.3 μM $CuCl_2$, respectively. For nutrient shift experiments, *Synechocystis* wild-type cells were initially cultivated in shaking flasks with 100 ml of BG-11 medium containing 50 mM $NaHCO_3$ to an optical density at 730 nm (OD_{730}) of ~0.2. The culture suspension was fast filtered with a nitrocellulose membrane filter (0.45-μm pore size, Millipore) that was mounted on a vacuum device (GM-0.33A, Jinteng, China) opened to a moderate level (*54*). Then, the cell pellets were rapidly washed and resuspended in 100 ml of pre-warmed (30°C) starvation medium lacking the indicated nutrient. After 6 hours of nitrogen deprivation or 12 hours of phosphorous or sulfur deprivation, the cultures were supplemented with 17.65 mM $NaNO_3$, 0.23 mM $Na_2HPO_4{\cdot}12H_2O$, and 0.31 mM Na_2SO_4, respectively. Samples were collected at the indicated time points after the nutrient addition. For comparative metabolomic analysis between different *Synechocystis* strains, cells were grown in shaking flasks with 100 ml of BG-11 medium to an OD_{730} of ~0.4.

Isotope-labeling experiments

The labeling compounds including uniformly ^{13}C- and ^{15}N-labeled arginine ([*U*-^{13}C, *U*-^{15}N]arginine) and [*U*-^{13}C]asparagine were ≥99% pure and purchased from Cambridge Isotope Laboratories. Isotope-labeling experiments were performed as reported previously (*55*). Briefly, cyanobacterial cells were grown in shake flasks with 100 ml of BG-11 medium to an OD_{730} of ~0.4. The culture was supplemented with 0.5 mM [*U*-^{13}C, *U*-^{15}N]arginine or 0.5 mM [*U*-^{13}C]asparagine. After 4 hours of incubation with the labeling substrates, cells were collected by fast filtration for metabolite analysis.

Metabolomics

Quenching of metabolism and metabolite extraction were performed as described previously (*56*). Briefly, approximate 3×10^8 cyanobacterial cells were collected by fast filtration, and metabolites were extracted by rapid transfer of the filter into −40°C 40:40:20 methanol/acetonitrile/water. For extraction of polyamines, the filter was transferred into −40°C 40:40:20 methanol/acetonitrile/water with 0.1 M $NH_3{\cdot}H_2O$. After incubation at −20°C for 20 min, the samples were centrifuged, and the supernatant was collected.

Cell extracts were analyzed by ultrahigh-performance LC (UltiMate 3000, Thermo Fisher) coupled to a quadrupole-orbitrap mass spectrometer (Q-Exactive, Thermo Fisher). To increase the coverage of metabolomic profiling, three different LC procedures were carried out. Polar metabolites were separated with a Luna NH2 column (100 mm–by–2 mm internal diameter, 3-μm particle size; Phenomenex) as described previously (*57*). The injection volume was 10 μl. The mass spectrometer was run in electrospray ionization–negative (ESI^-) mode. Nonpolar metabolites were separated by reverse-phase chromatography using an Acquity HSS T3 column (100 mm by 2 mm, 1.8 μm; Waters) (*58*). The injection volume was 5 μl. The mass spectrometer was operated in electrospray ionization–positive (ESI^+) mode. Polyamines were separated by normal-phase chromatography using an Xbridge Amide column (100 mm by 2.1 mm, 3.5 μm; Waters). The injection volume was 5 μl. The mobile phase A was 0.1% formic acid in water, and mobile phase B was 0.1% formic acid in acetonitrile. The column was maintained at 40°C with a flow rate of 0.3 ml min^{-1}, and the gradient of B was as follows: 0 min, 95%; 1 min, 95%; 14 min, 60%; 16 min, 10%; 21 min, 10%; 21.1 min, 95%; and 29 min, 95% B. The mass spectrometer was run in ESI^+ mode.

The parameters of mass spectrometer were set as follows: ion spray voltage, +3.5 kV/−3.0 kV; capillary temperature, 300°C; probe heater temperature, 350°C; and sheath and auxiliary gas, 40 and 10 arbitrary units, respectively. Mass spectra were acquired using full scan over 70 to 1000 *m*/*z* at 70,000 resolution, and the automatic gain control (AGC) target was set to 3×10^6 and 1×10^6 for ESI^+ and ESI^-, respectively. MS/MS spectra were acquired at 17,500 resolution; 1×10^5 AGC target level; 1.0 *m*/*z* isolation window; and stepped normalized collision energy of 20, 30, and 40%. Top six masses were selected for MS/MS per scan.

LC-MS raw data were converted to the mzML format using ProteoWizard (*59*), which were further processed by the MZmine software to generate a data matrix consisting of retention time, *m*/*z* value, and peak intensity (*60*). Metabolite identification was performed by matching retention time, accurate mass, and MS/MS spectra with commercially available standards (Sigma-Aldrich or MedChemExpress) or enzymatically synthesized compounds (see below). Metabolite concentrations were determined by using a calibration curve generated with varying concentrations of the chemical standard. Hierarchical-clustering analysis of time-dependent concentration changes in metabolites was performed using an R package pheatmap (version 1.0.12). Molecular networking of MS/MS spectra was performed using the Global Natural Product Social Molecular Networking platform (*61*). All the acquired MS/MS spectra were compared and grouped according to their similarity via the computation of a modified cosine score (*62*). Visualization of the output from molecular networking was carried out with Cytoscape 3.9.1 software (https://cytoscape.org) (*63*).

Mutant construction and complementation

Synechocystis mutants with gene knockout were constructed by replacing the coding region of the target gene with a kanamycin resistance cassette (*64*). For construction of complemented strains, the wild-type gene and a spectinomycin resistance cassette were expressed under the control of P_{psbA2} promoter and were integrated into a neutral site in the genome of the corresponding mutant (*65*). All the mutants and genetic complementation were verified by DNA sequencing, and segregation of all the strains was confirmed by polymerase chain reaction (PCR) analyses. The complete

list of strains, plasmids, and primers used in this study is shown in tables S2 and S3, respectively.

Protein expression and purification

Synechocystis genes encoding CAPADH, CAPADC, and APAUH were PCR-amplified from the genomic DNA. Site-directed mutagenesis for construction of CAPADH and APAUH variants was carried out using the Site-Directed Mutagenesis Kit (Transgene), and the primers are listed in table S3. The genes encoding CAPADH (WP_198804688) and APAUH (WP_198806637) in *Leptolyngbya* sp. BL0902 were amplified from the genomic DNA. Chemically synthesized (GenScript) genes included the genes encoding CAPADH from *D. vulgaris* (WP_010937725), *G. sulfurreducens* (WP_010943175), *B. uniformis* (WP_005831761), *D. radiodurans* (WP_010887895), *H. pylori* (WP_000557673), and *S. pneumoniae* (SPD_0812, WP_000088780); the genes encoding CASDH from *A. tumefaciens* (Atu4170) and CANSDH from *V. cholerae* (VC1624); and the genes encoding APAUH from *T. volcanium* (PDB, 3PZL; WP_010916796) and *D. vulgaris* (WP_010937728). These genes were cloned into the vector pET28a. The resulting plasmids for production of the C-terminal hexahistidine-tagged proteins were transformed into *Escherichia coli* BL21 (DE3) (Novagen). Protein overexpression and purification were performed as described previously (*66*).

Isolation and NMR analysis of CAPA and APA

For synthesis of CAPA, the reaction mixture (15 ml) contained 50 mM potassium phosphate buffer (pH 7.4), 5 mM agmatine, 20 mM homoserine, 2 mM $NADP^+$, 1 mM dithiothreitol, 500 μg of homoserine dehydrogenase from *Saccharomyces cerevisiae*, and 500 μg of purified CAPADH. For synthesis of APA, the reaction mixture (30 ml) contained 50 mM potassium phosphate buffer (pH 7.4), 5 mM agmatine, 20 mM homoserine, 2 mM $NADP^+$, 1 mM dithiothreitol, 25 μM PLP, 1000 μg of homoserine dehydrogenase, and 1000 μg of each of purified CAPADH and CAPADC. After incubation overnight, the mixtures were lyophilized and extracted in 3 ml of 40:40:20 methanol/acetonitrile/water with 0.1 M $NH_3{\cdot}H_2O$. The aqueous layer was collected and subjected to a preparative HPLC (1290 infinity II-6125, Agilent) equipped with an Xbridge Amide column (150 mm by 4.6 mm, 3.5 μm; Waters). The mobile phase A was 0.5% formic acid in water, and mobile phase B was 0.5% formic acid in acetonitrile. The column was maintained at 40°C with a solvent flow rate of 1 ml/min, and the gradient of B was as follows: 0 min, 95%; 4 min, 70%; 10 min, 60%; 11 min, 20%; 15 min, 20%; 15.1 min, 95%; and 24 min, 95% B. The fractions containing CAPA or APA were pooled, and the identity and purity were checked by LC-MS/MS as described above. CAPA concentration was assessed through complete conversion to APA by CAPADC. APA concentration was determined using the purified APAUH that can completely hydrolyze the APA, and the formed urea was measured by the diacetyl monoxime colorimetric method (*67*).

NMR spectra were obtained with a Bruker Avance III HD (400 MHz) spectrometer. Samples were dried under reduced pressure and redissolved in D_2O. For both CAPA and APA, ^{1}H-NMR, ^{13}C-NMR, ^{1}H-^{1}H correlation spectroscopy, heteronuclear single-quantum coherence, and heteronuclear multiple-bond correlation spectra were recorded and analyzed using the MestReNova 14.0.0. The acquired ^{1}H and ^{13}C NMR signals were compared to those reported for the chemically synthesized APA (*37*). ASA was chemically synthesized as previously reported (*16*, *68*) and confirmed by ^{1}H-NMR [400 MHz, D_2O: δ 5.37 to 5.28 (m, 1H, 4-H), 4.21 to 4.13 (m, 1H, 2-H), 2.35 to 2.22 (m, 1H, 3-H), and 2.22 to 2.11 (m, 1H, 3-H)].

Enzyme assays

The three-step conversion of agmatine to spermidine via the CAPA pathway was reconstituted in vitro by addition of a mixture of the purified CAPADH, CAPADC, and APAUH (5 μg each) to 200 μl of 50 mM potassium phosphate buffer (pH 7.4) containing 5 mM agmatine, 20 mM homoserine, 2 mM $NADP^+$, 1 mM dithiothreitol, 25 μM PLP, and 5 μg of homoserine dehydrogenase. Various combinations of CAPADH, CAPADC, and APAUH were tested to confirm that the presence of all three enzymes is required. Polyamines produced by the enzymatic reactions were identified by HPLC following derivatization with phenylisothiocyanate (*66*) and were further validated by LC-MS/MS as described above.

The CAPADH activity was determined by addition of 0.5 μg of the purified enzyme to 200 μl of 50 mM potassium phosphate buffer (pH 7.4) containing 5 mM agmatine, 1.25 mM chemically synthesized ASA, 0.25 mM NADPH, and 1 mM dithiothreitol. The change in NADPH absorbance was monitored at 340 nm with a Microplate spectrophotometer (PowerWave XS2, BioTek). Kinetics for agmatine were measured with 1.25 mM ASA and 0.25 mM NADPH; kinetics for NADPH or NADH were measured with 1.25 mM ASA and 5 mM agmatine. To test substrate specificity, agmatine was replaced by the same concentration of putrescine, 1,3-diaminopropane, cadaverine, and spermidine in the assay mixture. Kinetics of the enzyme toward putrescine and 1,3-diaminopropane were measured with 1.25 mM ASA and 0.25 mM NADPH. The apparent k_{cat} and K_m values were determined with GraphPad Prism.

The CAPADC activity was assayed by coupling the formation of CO_2 to the oxidation of NADH to NAD^+ through phosphoenolpyruvate carboxylase (PEPC) and malate dehydrogenase (MDH). Briefly, 0.5 μg of the purified enzyme was added to 200 μl of 50 mM tris-HCl buffer (pH 7.4) containing 2 mM purified CAPA, 25 μM PLP, 2.5 U of PEPC, and 2 U of MDH. The change in NADH absorbance was monitored at 340 nm. Kinetics for CAPA were measured with its concentration varying from 0.05 to 2 mM. To test substrate specificity, CAPA was replaced by the same concentration of ornithine, arginine, lysine, and *meso*-diaminopimelate in the assay mixture. To assess the activity toward carboxyspermidine, the reaction mixture containing putrescine, ASA, NADPH, and CASDH from *A. tumefaciens* was incubated overnight, and, then, the purified CAPADC was added to the mixture. The activity toward carboxynorspermidine was assessed by adding CAPADC to the reaction mixture containing 1,3-diaminopropane, ASA, NADPH, and CANSDH from *V. cholerae*.

The APAUH activity was determined by addition of 0.5 μg of the purified enzyme to 200 μl of tris-HCl buffer (pH 7.4), containing 5 mM APA. The formed urea was analyzed with the diacetyl monoxime colorimetric method or by GC-MS after derivatization with *N*-methyl-*N*-[*tert*-butyldimethylsilyl] trifluoroacetamide (Sigma-Aldrich) (*69*). The metal content in the APAUH was measured using inductively coupled plasma (ICP)–MS (NexION 300D, PerkinElmer) (*70*). Kinetics for APA were measured with its concentration varying from 0.05 to 5 mM. To test substrate specificity, APA was replaced by the same concentration of L-arginine, agmatine,

CAPA, guanidine, guanidinobutyrate, and guanidinopropionate in the assay mixture.

Homology modeling and molecular docking of enzymes

Homology modeling of *Synechocystis* CAPADH, CAPADC, and APAUH was performed by using Modeller (version 10.4) (*71*). For CAPADH, the structure of NADPH-complexed SPD_0812 from *S. pneumoniae* (PDB, 4RL6) was used as the reference, which was annotated as saccharopine dehydrogenase but was identified as a CAPADH based on biochemical analysis of the purified recombinant protein in this study (see fig. S14B). The homology model of CAPADC was constructed on the basis of the structure of PLP-bound carboxynorspermidine or CASDC from *C. jejuni* (PDB, 3 N29). For APAUH, the structure of the two Mn^{2+} ions-bound ureohydrolase from *T. volcanium* (PDB, 3PZL) was used as the reference, which was biochemically characterized as an APAUH in this study (see fig. S13A).

AutoDockTools (version 1.5.7) and AutoDock Vina (version 1.1.2) were used to prepare the protein structures and substrates and to perform molecular docking (*72*). The grid box in the docking procedure were defined to encompass the corresponding residues appeared in the substrate binding pocket of crystal structures for homologous proteins. All the structural graphics were generated with PyMOL (www.pymol.org).

Phylogenetic analysis of CAPADH and APAUH

Sequences of CAPADH and its orthologs and other saccharopine dehydrogenase family proteins (Pfam, PF16653) including CASDH, CANSDH, SR, LysDH, and HSS were aligned using MUSCLE (*73*), and phylogenetic tree was generated by Molecular Evolutionary Genetics Analysis version 7.0 (*74*) and visualized using Interactive Tree Of Life (*75*). A total of 31,294 proteins from the saccharopine dehydrogenase family were used for generation of a sequence similarity network (SSN) using the EFI-EST web tool (*76*). In this SSN, connected sequences with more than 80% identity are clustered into nodes, and nodes with more than 55% identity are connected by edges. The SSN was visualized with Cytoscape 3.9.1.

For phylogenetic analysis of APAUH, 208 protein sequences from the ureohydrolase superfamily (Pfam, PF00491), which includes APAUH, arginase, agmatine ureohydrolase, guanidine hydrolase, proclavaminate amidinohydrolase, formiminoglutamase, guanidinobutyrase, and guanidinopropionase, were aligned by Multiple Alignment using Fast Fourier Transform (MAFFT), and phylogenetic tree was reconstructed by W-IQ-TREE (*77*).

Distribution of the CAPA-pathway genes in bacterial genomes and metagenomes

CAPADH orthologs were identified using BLASTP with a stringency of 70% or more coverage and 47% or more identity to *Synechocystis* CAPADH. CAPADC homologs were searched in CAPADH-encoded genomes, with >35% sequence identity to *Synechocystis* CAPADC. APAUH orthologs were identified using 80% coverage and 30% identity to *Synechocystis* APAUH or 80% coverage and 35% identity to *T. volcanium* APAUH as the cutoff. A total of 16,546 reference and representative genomes of bacterial species were downloaded from the RefSeq database at NCBI (www.ncbi.nlm.nih.gov/refseq/) and screened for the CAPA-pathway genes. The MicrobesOnline database (www.microbesonline.org/) (*78*) and GenomeExplorer software (*79*) were used for analysis of genomic contexts for CAPADH. The ecological distribution data of 1546 bacterial strains with the CAPA-pathway genes were obtained from the Genomes OnLine Database (https://gold.jgi.doe.gov/) (*80*) and Bacterial and Viral Bioinformatics Resource Center (www.bv-brc.org/) (*81*).

Metagenome-assembled genomes were downloaded from the European Nucleotide Archive (www.ebi.ac.uk/ena) (*82*), which include 254 fecal metagenomes of healthy individuals from three countries on different continents (project accession numbers PRJEB26924, n = 97; PRJEB26097, n = 47; PRJEB33766, n = 110), 199 marine metagenomes of samples collected at different locations and depths (PRJEB46046, n = 114; PRJEB47400, n = 85), and 44 freshwater metagenomes (PRJEB36523, n = 32; PRJEB22516, n = 12). All identified proteins of these metagenomes were searched against *Synechocystis* CAPADH using DIAMOND (*83*) BLASTP with a cutoff value of 1×10^{-60}. The resulting hits were filtered using the following criteria: at least 50% of the query sequence covered, and the residue E228 or both N104 and F113 residues present.

Statistics

Unless noted otherwise, data are presented as the means ± SD of n independent experiments, and P values were calculated with two-tailed Student's t test.

Supplementary Materials

This PDF file includes:
Figs S1 to S15
Legends for tables S1 to S3

Other Supplementary Material for this manuscript includes the following:
Table S1 to S3

REFERENCES AND NOTES

1. L. Miller-Fleming, V. Olin-Sandoval, K. Campbell, M. Ralser, Remaining mysteries of molecular biology: The role of polyamines in the cell. *J. Mol. Biol.* **427**, 3389–3406 (2015).
2. A. E. Pegg, Functions of polyamines in mammals. *J. Biol. Chem.* **291**, 14904–14912 (2016).
3. M. H. Park, E. C. Wolff, Hypusine, a polyamine-derived amino acid critical for eukaryotic translation. *J. Biol. Chem.* **293**, 18710–18718 (2018).
4. A. O. Gevrekci, The roles of polyamines in microorganisms. *World J. Microbiol. Biotechnol.* **33**, 204 (2017).
5. D. Chen, Q. Shao, L. Yin, A. Younis, B. Zheng, Polyamine function in plants: Metabolism, regulation on development, and roles in abiotic stress responses. *Front. Plant Sci.* **9**, 1945 (2018).
6. A. J. Michael, Polyamine function in archaea and bacteria. *J. Biol. Chem.* **293**, 18693–18701 (2018).
7. A. J. Michael, Biosynthesis of polyamines and polyamine-containing molecules. *Biochem. J.* **473**, 2315–2329 (2016).
8. H. Tabor, S. M. Rosenthal, C. W. Tabor, The biosynthesis of spermidine and spermine from putrescine and methionine. *J. Biol. Chem.* **233**, 907–914 (1958).
9. A. E. Pegg, *S*-Adenosylmethionine decarboxylase. *Essays Biochem.* **46**, 25–45 (2009).
10. H. Wu, J. Min, Y. Ikeguchi, H. Zeng, A. Dong, P. Loppnau, A. E. Pegg, A. N. Plotnikov, Structure and mechanism of spermidine synthases. *Biochemistry* **46**, 8331–8339 (2007).
11. K. Hamana, Polyamine distribution patterns in aerobic Gram-positive cocci and some radio-resistant bacteria. *J. Gen. Appl. Microbiol.* **40**, 181–195 (1994).
12. R. Hosoya, K. Hamana, Distribution of two triamines, spermidine and homospermidine, and an aromatic amine, 2-phenylethylamine, within the phylum Bacteroidetes. *J. Gen. Appl. Microbiol.* **50**, 255–260 (2004).

13. C. C. Hanfrey, B. M. Pearson, S. Hazeldine, J. Lee, D. J. Gaskin, P. M. Woster, M. A. Phillips, A. J. Michael, Alternative spermidine biosynthetic route is critical for growth of *Campylobacter jejuni* and is the dominant polyamine pathway in human gut microbiota. *J. Biol. Chem.* **286**, 43301–43312 (2011).
14. G. H. Tait, A new pathway for the biosynthesis of spermidine. *Biochem. Soc. Trans.* **4**, 610–612 (1976).
15. S. H. Kim, Y. Wang, M. Khomutov, A. Khomutov, C. Fuqua, A. J. Michael, The essential role of spermidine in growth of *Agrobacterium tumefaciens* is determined by the 1,3-diaminopropane moiety. *ACS Chem. Biol.* **11**, 491–499 (2016).
16. X. Liang, H. Deng, T. Xiong, Y. Bai, T. P. Fan, X. Zheng, Y. Cai, Overexpression and biochemical characterization of a carboxyspermidine dehydrogenase from *Agrobacterium fabrum* str. C58 and its application to carboxyspermidine production. *J. Sci. Food Agric.* **102**, 3858–3868 (2022).
17. S. Yamamoto, K. Hamanaka, Y. Suemoto, B. Ono, S. Shinoda, Evidence for the presence of a novel biosynthetic pathway for norspermidine in *Vibrio*. *Can. J. Microbiol.* **32**, 99–103 (1986).
18. H. Nakao, S. Shinoda, S. Yamamoto, Purification and some properties of carboxynorspermidine synthase participating in a novel biosynthetic pathway for norspermidine in *Vibrio alginolyticus*. *J. Gen. Microbiol.* **137**, 1737–1742 (1991).
19. J. Lee, V. Sperandio, D. E. Frantz, J. Longgood, A. Camilli, M. A. Phillips, A. J. Michael, An alternative polyamine biosynthetic pathway is widespread in bacteria and essential for biofilm formation in *Vibrio cholerae*. *J. Biol. Chem.* **284**, 9899–9907 (2009).
20. A. A. Bridges, B. L. Bassler, Inverse regulation of *Vibrio cholerae* biofilm dispersal by polyamine signals. *eLife* **10**, e65487 (2021).
21. J. F. Qin, A. Krivoruchko, B. Y. Ji, Y. Chen, M. Kristensen, E. Ozdemir, J. D. Keasling, M. K. Jensen, J. Nielsen, Engineering yeast metabolism for the discovery and production of polyamines and polyamine analogues. *Nat. Catal.* **4**, 498–509 (2021).
22. M. Y. Chen, W. K. Teng, L. Zhao, C. X. Hu, Y. K. Zhou, B. P. Han, L. R. Song, W. S. Shu, Comparative genomics reveals insights into cyanobacterial evolution and habitat adaptation. *ISME J.* **15**, 211–227 (2021).
23. P. Flombaum, J. L. Gallegos, R. A. Gordillo, J. Rincon, L. L. Zabala, N. Jiao, D. M. Karl, W. K. Li, M. W. Lomas, D. Veneziano, C. S. Vera, J. A. Vrugt, A. C. Martiny, Present and future global distributions of the marine Cyanobacteria *Prochlorococcus* and *Synechococcus*. *Proc. Natl. Acad. Sci. U.S.A.* **110**, 9824–9829 (2013).
24. M. M. M. Kuypers, H. K. Marchant, B. Kartal, The microbial nitrogen-cycling network. *Nat. Rev. Microbiol.* **16**, 263–276 (2018).
25. S. Jantaro, H. Kidron, D. Chesnel, A. Incharoensakdi, P. Mulo, T. Salminen, P. Maenpaa, Structural modeling and environmental regulation of arginine decarboxylase in Synechocystis sp. PCC 6803. *Arch. Microbiol.* **184**, 397–406 (2006).
26. K. Kera, T. Nagayama, K. Nanatani, C. Saeki-Yamoto, A. Tominaga, S. Souma, N. Miura, K. Takeda, S. Kayamori, E. Ando, K. Higashi, K. Igarashi, N. Uozumi, Reduction of spermidine content resulting from inactivation of two arginine decarboxylases increases biofilm formation in *Synechocystis* sp. strain PCC 6803. *J. Bacteriol.* **200**, e00664-17 (2018).
27. X. Zhu, Q. Li, C. Yin, X. Fang, X. Xu, Role of spermidine in overwintering of cyanobacteria. *J. Bacteriol.* **197**, 2325–2334 (2015).
28. M. J. Quintero, A. M. Muro-Pastor, A. Herrero, E. Flores, Arginine catabolism in the Cyanobacterium *Synechocystis* sp. Strain PCC 6803 involves the urea cycle and arginase pathway. *J. Bacteriol.* **182**, 1008–1015 (2000).
29. B. Wang, Y. Xu, X. Wang, J. S. Yuan, C. H. Johnson, J. D. Young, J. Yu, A guanidine-degrading enzyme controls genomic stability of ethylene-producing cyanobacteria. *Nat. Commun.* **12**, 5150 (2021).
30. K. Samasil, L. Lopes de Carvalho, P. Maenpaa, T. A. Salminen, A. Incharoensakdi, Biochemical characterization and homology modeling of polyamine oxidase from cyanobacterium Synechocystis sp. PCC 6803. *Plant Physiol. Biochem.* **119**, 159–169 (2017).
31. A. K. Vashishtha, A. H. West, P. F. Cook, Overall kinetic mechanism of saccharopine dehydrogenase (L-Glutamate forming) from *Saccharomyces cerevisiae*. *Biochemistry* **47**, 5417–5423 (2008).
32. K. Y. Ko, S. C. Park, S. Y. Cho, S. I. Yoon, Structural analysis of carboxyspermidine dehydrogenase from *Helicobacter pylori*. *Biochem. Biophys. Res. Commun.* **635**, 210–217 (2022).
33. D. F. Lee, N. Atencio, S. Bouchey, M. R. Shoemaker, J. S. Dodd, M. Satre, K. A. Miller, J. S. McFarlane, Kinetic and structural characterization of carboxyspermidine dehydrogenase of polyamine biosynthesis. *J. Biol. Chem.* **299**, 105033 (2023).
34. E. Johansson, J. J. Steffens, Y. Lindqvist, G. Schneider, Crystal structure of saccharopine reductase from *Magnaporthe grisea*, an enzyme of the alpha-aminoadipate pathway of lysine biosynthesis. *Structure* **8**, 1037–1047 (2000).
35. A. K. Vashishtha, A. H. West, P. F. Cook, Chemical mechanism of saccharopine reductase from *Saccharomyces cerevisiae*. *Biochemistry* **48**, 5899–5907 (2009).
36. X. Deng, J. Lee, A. J. Michael, D. R. Tomchick, E. J. Goldsmith, M. A. Phillips, Evolution of substrate specificity within a diverse family of beta/alpha-barrel-fold basic amino acid decarboxylases: X-ray structure determination of enzymes with specificity for L-arginine and carboxynorspermidine. *J. Biol. Chem.* **285**, 25708–25719 (2010).
37. M. Ohnuma, Y. Terui, M. Tamakoshi, H. Mitome, M. Niitsu, K. Samejima, E. Kawashima, T. Oshima, N^1-aminopropylagmatine, a new polyamine produced as a key intermediate in polyamine biosynthesis of an extreme Thermophile, Thermus thermophilus. *J. Biol. Chem.* **280**, 30073–30082 (2005).
38. N. Morimoto, W. Fukuda, N. Nakajima, T. Masuda, Y. Terui, T. Kanai, T. Oshima, T. Imanaka, S. Fujiwara, Dual biosynthesis pathway for longer-chain polyamines in the hyperthermophilic archaeon *Thermococcus kodakarensis*. *J. Bacteriol.* **192**, 4991–5001 (2010).
39. M. Ohnuma, T. Ganbe, Y. Terui, M. Niitsu, T. Sato, N. Tanaka, M. Tamakoshi, K. Samejima, T. Kumasaka, T. Oshima, Crystal structures and enzymatic properties of a triamine/agmatine aminopropyltransferase from *Thermus thermophilus*. *J. Mol. Biol.* **408**, 971–986 (2011).
40. M. C. Bewley, P. D. Jeffrey, M. L. Patchett, Z. F. Kanyo, E. N. Baker, Crystal structures of *Bacillus caldovelox* arginase in complex with substrate and inhibitors reveal new insights into activation, inhibition and catalysis in the arginase superfamily. *Structure* **7**, 435–448 (1999).
41. J. E. Jones, C. J. Dreyton, H. Flick, C. P. Causey, P. R. Thompson, Mechanistic studies of agmatine deiminase from multiple bacterial species. *Biochemistry* **49**, 9413–9423 (2010).
42. M. Piotrowski, T. Janowitz, H. Kneifel, Plant C-N hydrolases and the identification of a plant *N*-carbamoylputrescine amidohydrolase involved in polyamine biosynthesis. *J. Biol. Chem.* **278**, 1708–1712 (2003).
43. A. J. Michael, Evolution of biosynthetic diversity. *Biochem. J.* **474**, 2277–2299 (2017).
44. E. Albers, Metabolic characteristics and importance of the universal methionine salvage pathway recycling methionine from 5′-methylthioadenosine. *IUBMB Life* **61**, 1132–1142 (2009).
45. F. L. Shaw, K. A. Elliott, L. N. Kinch, C. Fuell, M. A. Phillips, A. J. Michael, Evolution and multifarious horizontal transfer of an alternative biosynthetic pathway for the alternative polyamine *sym*-homospermidine. *J. Biol. Chem.* **285**, 14711–14723 (2010).
46. J. W. Shaw, D. H. Grayson, I. Rozas, "Synthesis of guanidines and some of their biological applications" in *Guanidines as Reagents and Catalysts I* (Springer, 2015), chap. 174, pp. 1–51.
47. S. H. Kim, D. Semenya, D. Castagnolo, Antimicrobial drugs bearing guanidine moieties: A review. *Eur. J. Med. Chem.* **216**, 113293 (2021).
48. K. Igarashi, K. Kashiwagi, H. Hamasaki, A. Miura, T. Kakegawa, S. Hirose, S. Matsuzaki, Formation of a compensatory polyamine by *Escherichia coli* polyamine-requiring mutants during growth in the absence of polyamines. *J. Bacteriol.* **166**, 128–134 (1986).
49. T. Yoshida, A. Sakamoto, Y. Terui, K. Takao, Y. Sugita, K. Yamamoto, A. Ishihama, K. Igarashi, K. Kashiwagi, Effect of spermidine analogues on cell growth of *Escherichia coli* polyamine requiring mutant MA261. *PLOS ONE* **11**, e0159494 (2016).
50. A. J. Potter, J. C. Paton, Spermidine biosynthesis and transport modulate pneumococcal autolysis. *J. Bacteriol.* **196**, 3556–3561 (2014).
51. M. Sakanaka, Y. Sugiyama, A. Kitakata, T. Katayama, S. Kurihara, Carboxyspermidine decarboxylase of the prominent intestinal microbiota species *Bacteroides thetaiotaomicron* is required for spermidine biosynthesis and contributes to normal growth. *Amino Acids* **48**, 2443–2451 (2016).
52. M. Sakanaka, Y. Sugiyama, M. Nara, A. Kitakata, S. Kurihara, Functional analysis of arginine decarboxylase gene *speA* of *Bacteroides dorei* by markerless gene deletion. *FEMS Microbiol. Lett.* **365**, 10.1093/femsle/fny003, (2018).
53. R. Y. Stanier, R. Kunisawa, M. Mandel, G. Cohen-Bazire, Purification and properties of unicellular blue-green algae (order *Chroococcales*). *Bacteriol. Rev.* **35**, 171–205 (1971).
54. B. D. Bennett, J. Yuan, E. H. Kimball, J. D. Rabinowitz, Absolute quantitation of intracellular metabolite concentrations by an isotope ratio-based approach. *Nat. Protoc.* **3**, 1299–1311 (2008).
55. L. You, B. Berla, L. He, H. B. Pakrasi, Y. J. Tang, ^{13}C-MFA delineates the photomixotrophic metabolism of *Synechocystis* sp. PCC 6803 under light- and carbon-sufficient conditions. *Biotechnol. J.* **9**, 684–692 (2014).
56. J. D. Rabinowitz, E. Kimball, Acidic acetonitrile for cellular metabolome extraction from *Escherichia coli*. *Anal. Chem.* **79**, 6167–6173 (2007).
57. H. Zhang, Y. Liu, X. Nie, L. Liu, Q. Hua, G. P. Zhao, C. Yang, The cyanobacterial ornithine-ammonia cycle involves an arginine dihydrolase. *Nat. Chem. Biol.* **14**, 575–581 (2018).
58. F. Zheng, X. Zhao, Z. Zeng, L. Wang, W. Lv, Q. Wang, G. Xu, Development of a plasma pseudotargeted metabolomics method based on ultra-high-performance liquid chromatography-mass spectrometry. *Nat. Protoc.* **15**, 2519–2537 (2020).
59. M. C. Chambers, B. Maclean, R. Burke, D. Amodei, D. L. Ruderman, S. Neumann, L. Gatto, B. Fischer, B. Pratt, J. Egertson, K. Hoff, D. Kessner, N. Tasman, N. Shulman, B. Frewen, T. A. Baker, M. Y. Brusniak, C. Paulse, D. Creasy, L. Flashner, K. Kani, C. Moulding, S. L. Seymour, L. M. Nuwaysir, B. Lefebvre, F. Kuhlmann, J. Roark, P. Rainer, S. Detlev, T. Hemenway, A. Huhmer, J. Langridge, B. Connolly, T. Chadick, K. Holly, J. Eckels, E. W. Deutsch, R. L. Moritz, J. E. Katz, D. B. Agus, M. MacCoss, D. L. Tabb, P. Mallick, A cross-platform toolkit for mass spectrometry and proteomics. *Nat. Biotechnol.* **30**, 918–920 (2012).

60. R. Schmid, S. Heuckeroth, A. Korf, A. Smirnov, O. Myers, T. S. Dyrlund, R. Bushuiev, K. J. Murray, N. Hoffmann, M. Lu, A. Sarvepalli, Z. Zhang, M. Fleischauer, K. Duhrkop, M. Wesner, S. J. Hoogstra, E. Rudt, O. Mokshyna, C. Brungs, K. Ponomarov, L. Mutabdzija, T. Damiani, C. J. Pudney, M. Earll, P. O. Helmer, T. R. Fallon, T. Schulze, A. Rivas-Ubach, A. Bilbao, H. Richter, L. F. Nothias, M. Wang, M. Oresic, J. K. Weng, S. Bocker, A. Jeibmann, H. Hayen, U. Karst, P. C. Dorrestein, D. Petras, X. Du, T. Pluskal, Integrative analysis of multimodal mass spectrometry data in MZmine 3. *Nat. Biotechnol.* **41**, 447–449 (2023).
61. A. T. Aron, E. C. Gentry, K. L. McPhail, L. F. Nothias, M. Nothias-Esposito, A. Bouslimani, D. Petras, J. M. Gauglitz, N. Sikora, F. Vargas, J. J. J. van der Hooft, M. Ernst, K. B. Kang, C. M. Aceves, A. M. Caraballo-Rodriguez, I. Koester, K. C. Weldon, S. Bertrand, C. Roullier, K. Sun, R. M. Tehan, P. C. Boya, M. H. Christian, M. Gutierrez, A. M. Ulloa, J. A. Tejeda Mora, R. Mojica-Flores, J. Lakey-Beitia, V. Vasquez-Chaves, Y. Zhang, A. I. Calderon, N. Tayler, R. A. Keyzers, F. Tugizimana, N. Ndlovu, A. A. Aksenov, A. K. Jarmusch, R. Schmid, A. W. Truman, N. Bandeira, M. Wang, P. C. Dorrestein, Reproducible molecular networking of untargeted mass spectrometry data using GNPS. *Nat. Protoc.* **15**, 1954–1991 (2020).
62. J. Watrous, P. Roach, T. Alexandrov, B. S. Heath, J. Y. Yang, R. D. Kersten, M. van der Voort, K. Pogliano, H. Gross, J. M. Raaijmakers, B. S. Moore, J. Laskin, N. Bandeira, P. C. Dorrestein, Mass spectral molecular networking of living microbial colonies. *Proc. Natl. Acad. Sci. U.S.A.* **109**, E1743–E1752 (2012).
63. P. Shannon, A. Markiel, O. Ozier, N. S. Baliga, J. T. Wang, D. Ramage, N. Amin, B. Schwikowski, T. Ideker, Cytoscape: A software environment for integrated models of biomolecular interaction networks. *Genome Res.* **13**, 2498–2504 (2003).
64. J. G. K. Williams, [85] Construction of specific mutations in photosystem II photosynthetic reaction center by genetic engineering methods in *Synechocystis* 6803. *Meth. Enzymol.* **167**, 766–778 (1988).
65. K. A. Selim, M. Haffner, M. Burkhardt, O. Mantovani, N. Neumann, R. Albrecht, R. Seifert, L. Kruger, J. Stulke, M. D. Hartmann, M. Hagemann, K. Forchhammer, Diurnal metabolic control in cyanobacteria requires perception of second messenger signaling molecule c-di-AMP by the carbon control protein SbtB. *Sci. Adv.* **7**, eabk0568 (2021).
66. D. Liu, C. Yang, The nitrogen-regulated response regulator NrrA controls cyanophycin synthesis and glycogen catabolism in the cyanobacterium *Synechocystis* sp. PCC 6803. *J. Biol. Chem.* **289**, 2055–2071 (2014).
67. M. Rahmatullah, T. R. Boyde, Improvements in the determination of urea using diacetyl monoxime; methods with and without deproteinisation. *Clin. Chim. Acta* **107**, 3–9 (1980).
68. D. W. Tudor, T. Lewis, D. J. Robins, Synthesis of the trifluoroacetate salt of aspartic acid β-semialdehyde, an intermediate in the biosynthesis of L-lysine, L-threonine, and L-methionine. *Synthesis* **1993**, 1061–1062 (1993).
69. W. Dong, X. Nie, H. Zhu, Q. Liu, K. Shi, L. You, Y. Zhang, H. Fan, B. Yan, C. Niu, L. D. Lyu, G. P. Zhao, C. Yang, Mycobacterial fatty acid catabolism is repressed by FdmR to sustain lipogenesis and virulence. *Proc. Natl. Acad. Sci. U.S.A.* **118**, e2019305118 (2021).
70. A. Cvetkovic, A. L. Menon, M. P. Thorgersen, J. W. Scott, F. L. Poole 2nd, F. E. Jenney Jr., W. A. Lancaster, J. L. Praissman, S. Shanmukh, B. J. Vaccaro, S. A. Trauger, E. Kalisiak, J. V. Apon, G. Siuzdak, S. M. Yannone, J. A. Tainer, M. W. W. Adams, Microbial metalloproteomes are largely uncharacterized. *Nature* **466**, 779–782 (2010).
71. A. Sali, T. L. Blundell, Comparative protein modelling by satisfaction of spatial restraints. *J. Mol. Biol.* **234**, 779–815 (1993).
72. S. Forli, R. Huey, M. E. Pique, M. F. Sanner, D. S. Goodsell, A. J. Olson, Computational protein-ligand docking and virtual drug screening with the AutoDock suite. *Nat. Protoc.* **11**, 905–919 (2016).
73. R. C. Edgar, MUSCLE: Multiple sequence alignment with high accuracy and high throughput. *Nucleic Acids Res.* **32**, 1792–1797 (2004).
74. S. Kumar, G. Stecher, K. Tamura, MEGA7: Molecular evolutionary genetics analysis version 7.0 for bigger datasets. *Mol. Biol. Evol.* **33**, 1870–1874 (2016).
75. I. Letunic, P. Bork, Interactive Tree Of Life (iTOL) v5: An online tool for phylogenetic tree display and annotation. *Nucleic Acids Res.* **49**, W293–W296 (2021).
76. R. Zallot, N. Oberg, J. A. Gerlt, The EFI web resource for genomic enzymology tools: Leveraging protein, genome, and metagenome databases to discover novel enzymes and metabolic pathways. *Biochemistry* **58**, 4169–4182 (2019).
77. J. Trifinopoulos, L. T. Nguyen, A. von Haeseler, B. Q. Minh, W-IQ-TREE: A fast online phylogenetic tool for maximum likelihood analysis. *Nucleic Acids Res.* **44**, W232–W235 (2016).
78. P. S. Dehal, M. P. Joachimiak, M. N. Price, J. T. Bates, J. K. Baumohl, D. Chivian, G. D. Friedland, K. H. Huang, K. Keller, P. S. Novichkov, I. L. Dubchak, E. J. Alm, A. P. Arkin, MicrobesOnline: An integrated portal for comparative and functional genomics. *Nucleic Acids Res.* **38**, D396–D400 (2010).
79. A. A. Mironov, N. P. Vinokurova, M. S. Gelfand, Software for analysis of bacterial genomes. *Mol. Biol.* **34**, 222–231 (2000).
80. A. Bernal, U. Ear, N. Kyrpides, Genomes OnLine Database (GOLD): A monitor of genome projects world-wide. *Nucleic Acids Res.* **29**, 126–127 (2001).
81. R. D. Olson, R. Assaf, T. Brettin, N. Conrad, C. Cucinell, J. J. Davis, D. M. Dempsey, A. Dickerman, E. M. Dietrich, R. W. Kenyon, M. Kuscuoglu, E. J. Lefkowitz, J. Lu, D. Machi, C. Macken, C. Mao, A. Niewiadomska, M. Nguyen, G. J. Olsen, J. C. Overbeek, B. Parrello, V. Parrello, J. S. Porter, G. D. Pusch, M. Shukla, I. Singh, L. Stewart, G. Tan, C. Thomas, M. VanOeffelen, V. Vonstein, Z. S. Wallace, A. S. Warren, A. R. Wattam, F. Xia, H. Yoo, Y. Zhang, C. M. Zmasek, R. H. Scheuermann, R. L. Stevens, Introducing the Bacterial and Viral Bioinformatics Resource Center (BV-BRC): A resource combining PATRIC, IRD and ViPR. *Nucleic Acids Res.* **51**, D678–D689 (2023).
82. R. Leinonen, R. Akhtar, E. Birney, L. Bower, A. Cerdeno-Tarraga, Y. Cheng, I. Cleland, N. Faruque, N. Goodgame, R. Gibson, G. Hoad, M. Jang, N. Pakseresht, S. Plaister, R. Radhakrishnan, K. Reddy, S. Sobhany, P. Ten Hoopen, R. Vaughan, V. Zalunin, G. Cochrane, The European nucleotide archive. *Nucleic Acids Res.* **39**, D28–D31 (2011).
83. B. Buchfink, K. Reuter, H. G. Drost, Sensitive protein alignments at tree-of-life scale using DIAMOND. *Nat. Methods* **18**, 366–368 (2021).

Acknowledgments: We thank X. Xu for providing *Leptolyngbya* sp. BL0902 strain; X. Xu, S. Wang, and W. Hu for technical assistance on hybrid quadrupole-orbitrap MS; Y. Zhang and W. Lan for guidance on NMR analysis; and Z. Fang and Z. Qi for help with ICP-MS measurement. **Funding:** This work was supported by the National Key Research and Development Program of China (2021YFA0909700), the National Natural Science Foundation of China (31925001, 31921006, and 32230060), and the Chinese Academy of Sciences (XDB27020000). **Author contributions:** H.X. performed most experiments, analyzed data, and wrote the manuscript. X.N. analyzed data, performed bioinformatics, and wrote the manuscript. F.G. contributed LC-MS analysis. X.L. contributed enzyme assays. H.L. contributed nutrient shift experiments. H.Z. contributed metabolomic analysis. Y.C. contributed biochemical analysis and discussion. C.Y. designed experiments, analyzed data, and wrote the manuscript. **Competing interests:** The authors declare that they have no competing interests. **Data and materials availability:** All data needed to evaluate the conclusions in the paper are present in the paper and/or the Supplementary Materials.

Submitted 23 July 2023
Accepted 22 September 2023
Published 25 October 2023
10.1126/sciadv.adj9075

Science Advances

A bacterial spermidine biosynthetic pathway via carboxyaminopropylagmatine

Huachao Xi, Xiaoqun Nie, Fang Gao, Xinxin Liang, Hu Li, Haiyan Zhou, Yujie Cai, and Chen Yang

Sci. Adv. **9** (43), eadj9075. DOI: 10.1126/sciadv.adj9075

Science Advances (ISSN 2375-2548) is published by the American Association for the Advancement of Science. 1200 New York Avenue NW, Washington, DC 20005. The title *Science Advances* is a registered trademark of AAAS.